Magnetochemistry **2015**, *1*, 17-27; doi:10.3390/magnetochemistry1010017

OPEN ACCESS

magnetochemistry

ISSN 2312-7481

www.mdpi.com/journal/magnetochemistry

Communication

Spin-Crossover Hysteresis of $[Fe^{II}(L_H^{iPr})_2(NCS)_2]$ (L_H^{iPr} = *N*-2-Pyridylmethylene-4-Isopropylaniline) Accompanied by Isopropyl Conformation Isomerism

Naotaka Mochida, Akifumi Kimura and Takayuki Ishida *

Department of Engineering Science, The University of Electro-Communications, Chofu, Tokyo 182-8585, Japan; E-Mails: mochida@ttf.pc.uec.ac.jp (N.M.); kimura@ttf.pc.uec.ac.jp (A.K.)

* Author to whom correspondence should be addressed; E-Mail: takayuki.ishida@uec.ac.jp; Tel./Fax: +81-42-443-5501.

Academic Editor: Guillem Aromí

Received: 31 October 2015 / Accepted: 16 November 2015 / Published: 20 November 2015

Abstract: $[Fe^{II}(L_H^{iPr})_2(NCS)_2]$ (L_H^{iPr} = *N*-2-pyridylmethylene-4-isopropylaniline) showed an abrupt spin-crossover (SCO) at $T_{1/2}\downarrow$ = 154 K on cooling and at $T_{1/2}\uparrow$ = 167 K on heating. The thermal hysteresis with a width of 13 K is related with the structural solid-state phase transition. The space group was unchanged as $P2_1/n$ with Z = 8, and there are two crystallographically independent molecules in a unit cell at 130 and 180 K. The two iron (II) sites synchronously underwent the SCO. The most drastic structural change across the SCO was found in the conformation isomerization of an isopropyl group. Namely, rotation around the $C(sp^2)$–$C(sp^3)$ bond by *ca.* 120° takes place during the SCO. There is no structural disorder in the high-temperature phase. The thermal hysteresis probably originates in the bulk isomerization requiring considerable activation energy in the crystalline solid.

Keywords: spin crossover; hysteresis; structural phase transition; order-disorder transition; conformational isomer; conformer; spin transition; crystal structure

1. Introduction

Spin-crossover (SCO) is a reversible transition between low-spin (LS) and high-spin (HS) states by external stimuli like heat, light, pressure, or magnetic field [1–15]. For development of multi-functional materials involving thermo- and photo-chromisms and -magnetisms, bistability exhibiting thermal

hysteresis is key [1–13]. SCO thermal hysteresis is often found to accompany a structural solid-state phase transition [16–20]. Iron (II) ($3d^6$) coordination compounds attract much attention in various SCO complexes, because crossover takes place between dia- and paramagnetic states to show drastic change in magnetic and chromic properties. The six-nitrogen donor structures (*i.e.*, $Fe^{II}N_6$) have been studied extensively [1–23], and in particular diimine ligands like 2-azaarylmethyleneimine derivatives are one of the most popular ligands for this purpose (Scheme 1) [21–23].

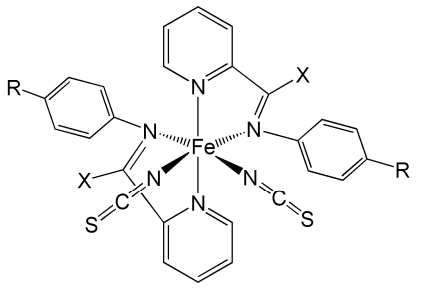

X = H; R = $CH(CH_3)_2$: $[Fe(L_H^{iPr})_2(NCS)_2]$
X = H; R = *n*-$C_{16}H_{33}$: $[Fe(L_H^{C16})_2(NCS)_2]$
X = 2-Py; R = *n*-$C_{16}H_{33}$: $[Fe(L_{Py}^{C16})_2(NCS)_2]$

Scheme 1. Structural formulas.

We have already reported that $[Fe(L_H^{C16})_2(NCS)_2]$ (L_H^{C16} = 4-hexadecyl-*N*-(2-pyridylmethylene)-aniline) exhibited SCO behavior with T_C = 176 K only after annealing above 353 K, which can be interpreted in terms of a metastable phase [24]. Another example has also been reported, where $[Fe(L_{Py}^{C16})_2(NCS)_2]$ (L_{Py}^{C16} = 4-hexadecyl-*N*-(di-2-pyridylmethylene)aniline) underwent SCO at $T_C\uparrow$ = 300 K and $T_C\downarrow$ = 210 K in the first thermal cycle only [25]. These SCO phenomena are supposed to interact with a metaphase transition [24,25], and it is rationalized by thinking of the role of the long alkyl chains. Unfortunately, there is only evidence from powder X-ray diffraction and thermal analysis for the mesophase transition. In the present study, small and branched alkyl groups have been introduced to the $[Fe(L)_2(NCS)_2]$ system, and single-crystal X-ray crystallographic analyses were attempted for a clue to possible structural phase transition. We will report here the SCO thermal hysteresis of $[Fe(L_H^{iPr})_2(NCS)_2]$ (L_H^{iPr} = *N*-2-pyridylmethylene-4-isopropylaniline) and discuss the origin of the hysteresis, based on the crystal structures determined in both LS and HS phases.

2. Results and Discussion

The specimen $[Fe(L_H^{iPr})_2(NCS)_2]$ was prepared according to the conventional method [21–25]. After the L_H^{iPr} was isolated and characterized, the complex formation was conducted in methanol using $FeCl_2$ and LiNCS as ion sources. The dark blue polycrystalline compound was isolated on a filter, and the product was subjected to X-ray crystal structure analysis and physical measurements without further purification. The elemental and spectroscopic analyses supported the composition formula of $[Fe(L_H^{iPr})_2(NCS)_2]$.

The magnetic susceptibilities of polycrystalline specimens of $[Fe(L_H^{iPr})_2(NCS)_2]$ were measured on a SQUID magnetometer in a temperature range of 10–300 K. As Figure 1 shows, the $\chi_m T$ value was 3.5 $cm^3\ K{\cdot}mol^{-1}$ at 300 K, being compatible with the S = 2 HS state of the iron(II) ion. On cooling, the $\chi_m T$ value abruptly decreased to practically null $\chi_m T$ at $T_{1/2}\downarrow$ = 154 K, and this phase is assigned to the

$S = 0$ LS state. The present complex showed thermal hysteresis. On heating, the $\chi_m T$ profile exhibited an upsurge at $T_{1/2}\uparrow$ = 167 K and traced the cooling curve above 170 K. Thus, the hysteresis width was 13 K. This SCO behavior was reproduced on repeated thermal cycles.

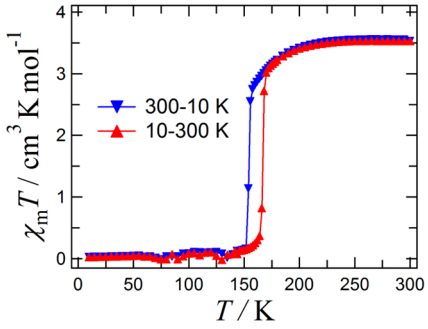

Figure 1. Temperature dependence of $\chi_m T$ for $[Fe(L_H{}^{iPr})_2(NCS)_2]$ measured at 5000 Oe.

The X-ray crystallographic analysis on $[Fe(L_H{}^{iPr})_2(NCS)_2]$ was successful below and above the SCO temperature (Figure 2), but owing to the microcracks occurred during the transition the final *R* factors in the low-temperature phase were slightly unsatisfactory (Table 1). The space group was unchanged as $P2_1/n$ with $Z = 8$, and there are two crystallographically independent molecules in a unit cell at 130 and 180 K. The unit cell was somewhat deformed on cooling, as indicated with the change of β (102.153(9)° at 130 K *vs.* 105.247(9)° at 180 K). The cell volume was shrunk by 3.0%, but interestingly the *b* length was elongated by 2.5%. This issue will be discussed later.

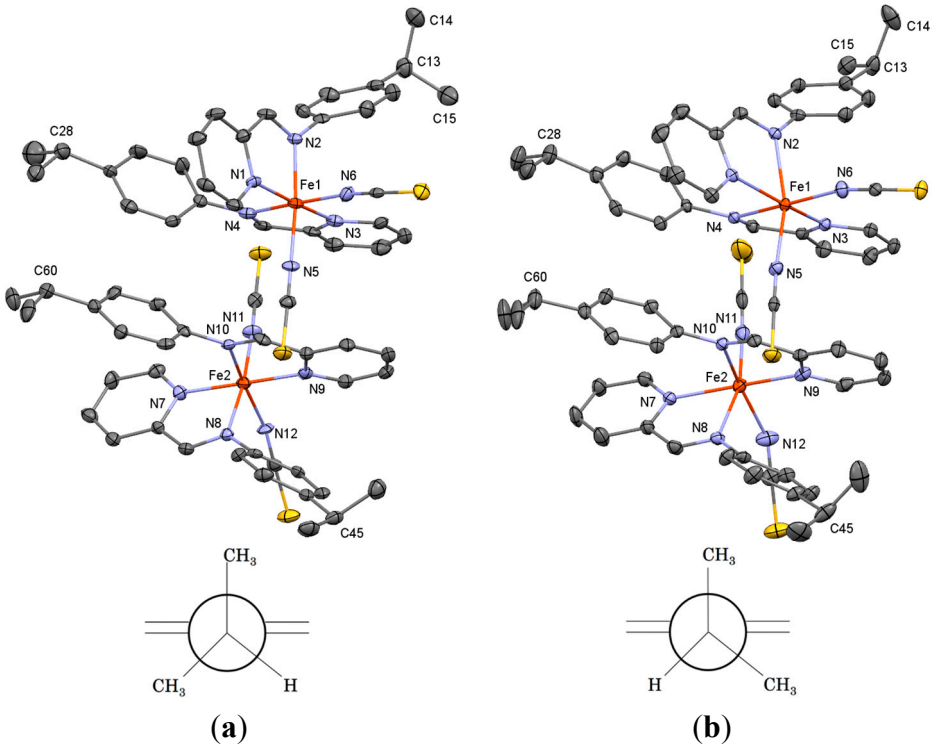

Figure 2. X-ray crystal structures of the asymmetric unit of of $[Fe(L_H{}^{iPr})_2(NCS)_2]$ in (**a**) the low-temperature phase measured at 130 K and (**b**) the high-temperature phase measured at 180 K. Schematic drawings of the conformation around the C14–C13–C15 isopropyl and phenyl groups are also shown.

Table 1. Selected crystallographic parameters of $[Fe(L_H^{iPr})_2(NCS)_2]$ measured at 130 and 180 K.

Formula	$C_{32}H_{32}FeN_6S_2$	$C_{32}H_{32}FeN_6S_2$
formula weight	620.61	620.61
T/K	130	180
crystal system	monoclinic	monoclinic
space group	$P2_1/n$	$P2_1/n$
a/Å	21.381(5)	21.521(5)
b/Å	12.668(3)	12.363(3)
c/Å	23.151(5)	24.605(4)
β/°	102.153(9)	105.247(9)
V/Å^3	6130(3)	6316(3)
Z	8	8
d_{calcd}/g·cm^{-3}	1.345	1.305
μ(MoKα)/mm^{-1}	0.660	0.640
number of total reflections	12913	14268
$R(F)$ ($I > 2\sigma(I)$) [a]	0.0983	0.0644
wR (F^2) (all reflections) [b]	0.1112	0.0690
goodness-of-fit parameter	1.157	1.185

[a] $R = \Sigma[|F_o| - |F_c|]/\Sigma|F_o|$; [b] $wR = [\Sigma w(F_o^2 - F_c^2)/\Sigma wF_o^4]^{1/2}$.

The asymmetric units determined at 130 and 180 K are drawn in Figure 2. Each iron (II) is coordinated with two diimines and two thiocyanates, affording an $Fe^{II}N_6$ coordination sphere. The molecular structures are similar to each other, and two thiocyanate groups are located at a *cis* position, as often seen in the $[Fe(L)_2(NCS)_2]$ family [21–25]. The two molecules are arranged so that two L_H^{iPr} fragments are pancake-type stacked with respect to the throughout benzylideneaniline π-conjugate system. The shortest interatomic distances are 3.510(10) Å ($C24_{Ph}\cdots C57_{Ph}$), 3.435(11) Å ($C18_{py}\cdots C50_{py}$), and 3.358(10) Å ($C21_{imine}\cdots C53_{imine}$) at 130 K, which are comparable to twice the van der Waals radius of carbon (3.4 Å) [26]. At 180 K, the shortest distances are 3.490(5) Å ($C24_{Ph}\cdots C57_{Ph}$), 3.500(5) Å ($C17_{py}\cdots C50_{py}$), and 3.460(4) Å ($C21_{imine}\cdots C53_{imine}$). The Fe–N coordination bonds at 130 K are shortened by 9.9% and 7.9% on average for Fe1 and Fe2, respectively, compared with those measured at 180 K (Table 2). This finding evidences the LS phase at 130 K and HS phase at 180 K. Furthermore, the SCO behavior at two iron (II) sites is synchronized, as the spin transition was quite sharp and no intermediate structure could be found inbetween. The π-π interaction seems to bring about the cooperative SCO at Fe1 and Fe2.

Table 2. Fe–N bond distances (d) in Å for $[Fe(L_H^{iPr})_2(NCS)_2]$ measured at 130 and 180 K.

d	**130 K**	**180 K**	***d***	**130 K**	**180 K**
Fe1–N1	1.953(6)	2.156(3)	Fe2–N7	1.971(7)	2.136(3)
Fe1–N2	1.946(6)	2.241(3)	Fe2–N8	1.968(6)	2.239(3)
Fe1–N3	1.956(6)	2.168(3)	Fe2–N9	1.958(7)	2.116(4)
Fe1–N4	1.969(7)	2.274(3)	Fe2–N10	1.964(6)	2.179(3)
Fe1–N5	1.943(6)	2.088(3)	Fe2–N11	1.934(7)	2.026(4)
Fe1–N6	1.942(7)	2.069(4)	Fe2–N12	1.956(6)	2.066(4)
Average	1.952	2.166	Average	1.959	2.127

One may point out that the bond angles around the Fe ions are relatively bent at 180 K. Actually, the *trans*-N–Fe–N(CS) bond angles at 180 K are smaller than those at 130 K by *ca.* 9° (Table 3). On elongating the Fe–N bonds, the coordination polyhedra are enlarged, and the Fe–N(CS) bond may be forced to bend and partially relieve the van der Waals interaction around the terminal sulfur atoms. The Fe–N–C(S) angles at 180 K are found to be bent as well, possibly owing to the same reason.

Table 3. *Trans*-N–Fe–N(CS) bond angles (θ) in degree for $[Fe(L_H^{iPr})_2(NCS)_2]$ measured at 130 and 180 K.

θ	130 K	180 K	θ	130 K	180 K
N2–Fe1–N5	173.3(3)	164.52(11)	N8–Fe2–N11	173.2(3)	165.18(13)
N4–Fe1–N6	174.5(3)	165.95(11)	N10–Fe2–N12	168.5(3)	159.38(13)
Average	173.9	165.2	Average	170.9	162.3

The dislocation of the atomic positions is basically small across the SCO, but from a close look at the N1–N2-involving L_H^{iPr} ligand, we can find that the phenyl ring is largely twisted. The torsion angles (ϕ) between the pyridine and benzene rings in the N1–N2 L_H^{iPr} are 99.0(3)° at 130 K while 51.7(1)° at 180 K. In three other L_H^{iPr} ligands, ϕ are 62.8(3), 55.6(3), and 53.7(3)° at 130 K and 56.8(1), 46.5(1), and 49.8(1)° at 180 K, for the N3–N4, N7–N8, and N9–N10 ligands, respectively. As a result, $\Delta\phi$ are 47, 6, 9, and 4°, respectively, for four L_H^{iPr} ligands. In short, only one L_H^{iPr} ligand experiences meaningful conformation change. The most drastic difference was found in the conformation of the C14–C13–C15 isopropyl group, while three other isopropyl groups hardly moved. The conformation is regulated with the steric effect from two methyl and one hydrogen groups at C13, and the rotation around the $C(sp^2)$–$C(sp^3)$ bond by *ca.* 120° would give at least three possible energy minima. Thus, the X-ray crystallographic analysis clarifies that the present spin transition is accompanied by the structural solid-state phase transition. It is reasonable that the thermal hysteresis would usually be found in the first-order phase transition.

The conformation energy profile of a mother compound isopropylbenzene (kumene) has been well investigated [27–30]. Theoretical computations suggested the conformation of the lowest energy as that in which the methine C–H group is situated coplanar to the phenyl ring, and agreed well with many experiments [27,28]. An apparent barrier of 6.5 $kJ \cdot mol^{-1}$ to rotation about the $C(sp^2)$–$C(sp^3)$ bond was characterized, determined by means of ^1H NMR technique in solution [28,29]. The microwave spectroscopy indicated that the barrier is only 0.8 $kJ \cdot mol^{-1}$ in a gas phase [30]. The experimental barriers for rotation around the $C(sp^2)$–$C(sp^3)$ bond seem controversial. However, it may be acceptable that the barrier depends on the phase where the measurements performed. The notable difference between the present work and the references [27–30] is that experimentally observed conformations (the bottom of Figure 2) violate the theoretical prediction. In the solid-state case like the present study, the barrier would be severely influenced by van der Waals interaction from surrounding molecules.

From the present experiments on $[Fe(L_H^{iPr})_2(NCS)_2]$, we found two stable conformers, as schematically expressed in the bottom of Figure 2. Since they are approximately in a mirror image, the preference of a stable conformer is determined from the intermolecular interaction in the crystalline solid. The C (sp^2)–$C(sp^3)$ bond of the C14–C13–C15 isopropyl group is arranged almost parallel in the *b* direction (Figure 3). This isopropyl group seems to accommodate the steric congestion increased on

cooling, being responsible for the negative shrinkage factor of the *b* axis (see above). The C13 (methine)···S3$^{\#}$ interatomic distance of 4.38(1) Å at 130 K may afford a clue to the present steric effect (the symmetry operation code for # is 1 − *x*, 1 − *y*, 1 − *z*). The two methyl groups C14 and C15 are located away from S3$^{\#}$ because of the van der Waals repulsive interaction. At 180 K, the C13···S3$^{\#}$ interatomic distance becomes as long as 5.100(6) Å, and a methyl group approaches S3$^{\#}$ with the C15···S3# distance of 3.824(5) Å, possibly owing to the van der Waals or hydrogen bond attractive interaction with S3$^{\#}$. Such intermolecular interactions must be much stronger than the internal one.

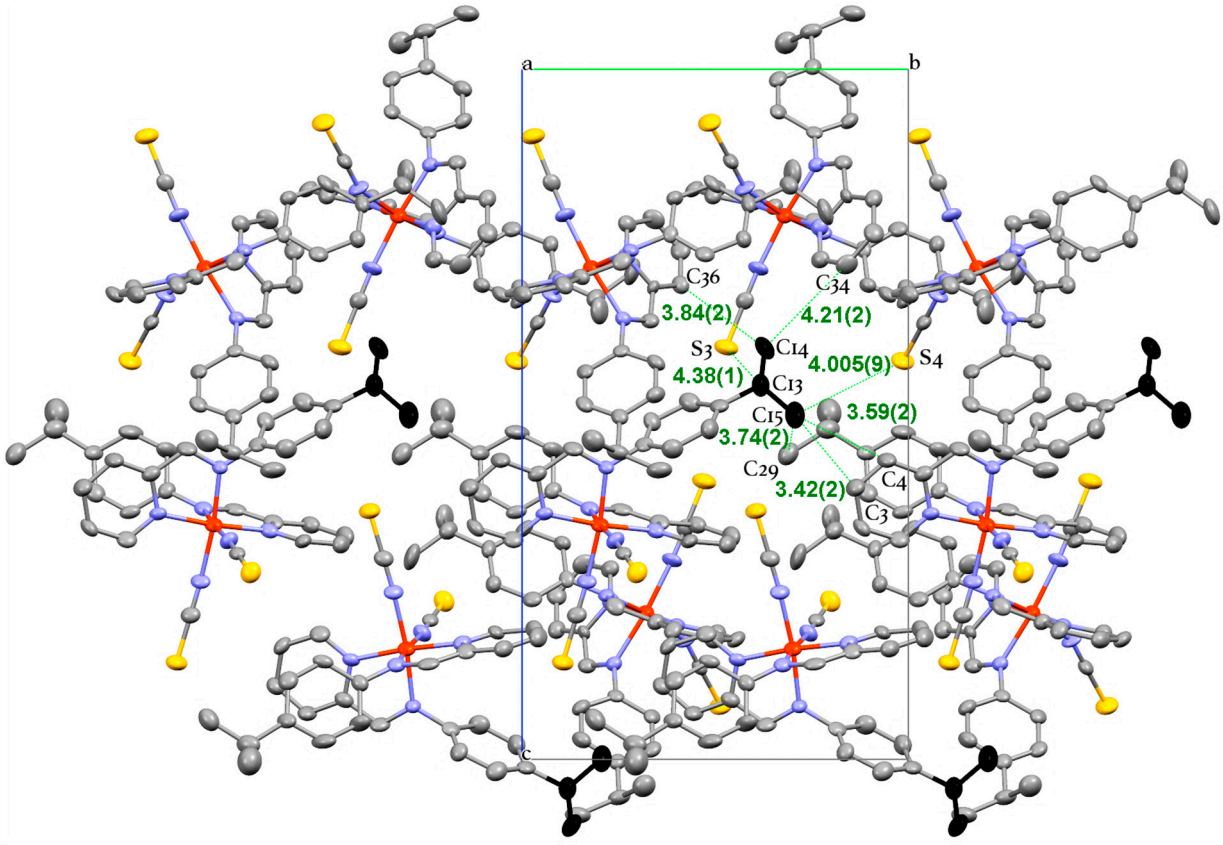

Figure 3. Molecular arrangement in the crystal of [Fe(L_H^{iPr})$_2$(NCS)$_2$] at 130 K, viewed along the *a* axis. The C14–C13–C15 isopropyl groups are highlighted. Selected intermolecular atomic distances are shown with dotted lines.

We have to stress that there is no disorder in the molecular structures determined. In the HT phase, attempts at the population analysis of scrambling two methyl and one hydrogen groups were unsuccessful. The residual electron density in the differential Fourier map has a maximum 1.70 e^{-}/Å^3 and the residues are located near the iron and sulfur atoms. The present transition does not belong to a category of the disorder-order transition. Conformation isomerism is schematically explained in Figure 4, in connection with the energy profile. There have been increasing reports on hysteretic SCO materials coupled with order-disorder transition [16,17,31–33]. For example, [Fe(DAPP)(abpt)](ClO$_4$)$_2$ showed the structural phase transition involving ordered and disordered perchlorate configuration and the SCO hysteresis width of 10 K (DAPP = bis(3-aminopropyl)(2-pyridylmethyl)amine, abpt = 4-amino-3,5-bis(pyridin-2-yl)-1,2,4-triazole) [17]. A huge hysteresis width 40 K was recorded in [Fe(H$_4$L)$_2$](ClO$_4$)$_2$·H$_2$O·2(CH$_3$)$_2$CO, and multiple SCO steps involve combination of disorder positions

of perchlorate and acetone (H_4L = 2,6-bis[5-(2-hydroxyphenyl)pyrazol-3-yl]pyridine) [31]. The order-disorder structural phase transition is believed as a promising ingredient to the hysteretic SCO.

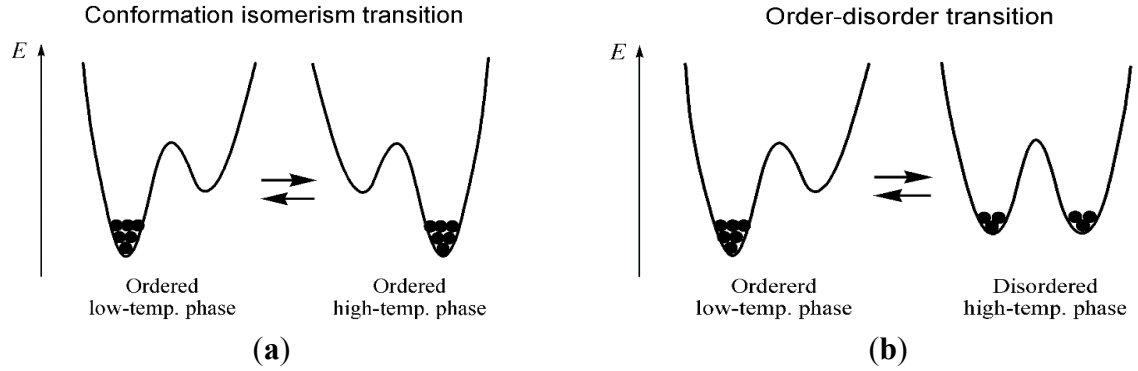

Figure 4. Schematic energy profiles of (**a**) conformation isomerism; and (**b**) order-disorder transition.

An *n*-alkyl conformation disorder was found in the SCO of $[Fe(ptz)_6](BF_4)_2$ with a hysteresis width of 7 K (ptz = 1-propyltetrazole) [32]. A very unique multi-stable SCO material was reported on $[Fe(nBu\text{-}im)_3(tren)](PF_6)_2$, which involves both disorders of *n*-butyl groups and counter anion PF_6 and showed 14 and 41 K hysteresis for two polymorphs ((nBu-im)$_3$(tren) = tris[2-(1-*n*-buty-1*H*-limidazol-2-ylmethyleneamino)ethyl]amine) [33]. These compounds involve short *n*-alkyl groups in common and attract attention as a prototype of higher alkyl analogs. On the other hand, $[Fe(L_H{}^{iPr})_2(NCS)_2]$ has a methyl-branched short alkyl group, and the factor of conformation preference is different from trans/gauche-type energy profile. The present case is rare, because methyl configuration is utilized and there is completely no disorder in the HS state of $[Fe(L_H{}^{iPr})_2(NCS)_2]$.

As described in the introduction, when completely irreversible mesophase transitions were coupled with the spin equilibrium system, irreversible spin-transition behavior was observed [24,25]. On the other hand, complete reversible spin transition systems belong to an opposing limit, giving spin equilibrium systems. We can imagine typical systems free from intermolecular interaction like solution systems [34–36] for the latter category. The present compound has a moderately bulky alkyl group and intermediate intermolecular interaction between the two limits. In other words, an activation energy just suitable for the structural phase transition seems to afford a hysteretic SCO system.

3. Experimental Section

3.1. Materials

The ligand $L_H{}^{iPr}$ and complex $[Fe(L_H{}^{iPr})_2(NCS)_2]$ was prepared according to the known procedure [37]. A clear methanol solution (5 mL) containing isopropylaniline (0.678 g; 5.0 mmol) and 2-formylpyridine (0.537 g; 5.0 mmol) was refluxed for 12 h. Concentration under reduced pressure quantitatively gave the condensed product *N*-2-pyridylmethylene-4-isopropylaniline ($L_H{}^{iPr}$) as yellow oil (1.10 g). ^{1}H NMR (500 MHz, $CDCl_3$) δ 8.71 (1H, dd, *J* = 1, 5 Hz), 8.63 (1H, s), 8.20 (1H, d, *J* = 8 Hz), 7.80 (1H, dt, *J* = 1, 8 Hz), 7.36 (1H, dd, *J* = 5, 8 Hz), 7.22–7.29 (4H, m), 2.95 (1H, septet, *J* = 7 Hz), 1.28 (6H, d, *J* = 7 Hz). ^{13}C NMR (126 MHz, $CDCl_3$) 159.79, 154.85, 149.76, 148.66, 147.87, 136.74, 127.33, 125.08, 121.91, 121.28, 33.86, 24.13. IR (neat, attenuated total reflection (ATR)) 2953,

2919, 1625, 1580, 1566, 1500, 1457, 1434, 1339, 1199, 1054, 992, 876, 842, 824, 783, 747, 615, 564, 406·cm^{-1}. A mixture of L_H^{iPr} (0.113 g; 0.50 mmol), $FeCl_2 \cdot 4H_2O$ (0.050 g; 0.25 mmol), LiNCS (0.0334 g; 0.51 mmol), and L-ascorbic acid (2.7 mg) in methanol (4 mL) was allowed to stand in a refrigerator for 24 h. Dark blue platelets of $[Fe(L_H^{iPr})_2(NCS)_2]$ were precipitated and separated. Yield 13%–33%. M.p. 201–202 °C. IR (neat, ATR) 2955, 2867, 2047, 1592, 1439, 1013, 818, 770, 569·cm^{-1}. Anal. Calcd. for $C_{32}H_{32}FeN_6S_2$: C, 61.93%; H, 5.20%; N, 13.54%; S, 10.33%. Found: C, 61.98%; H, 5.10%; N, 13.61%.

3.2. Crystallographic Analysis

X-ray diffraction data of $[Fe(L_H^{iPr})_2(NCS)_2]$ at 130 and 180 K were collected on Mercury CCD (Rigaku, Tokyo, Japan) and *R*-axis Rapid IP diffractometers (Rigaku, Tokyo, Japan) with graphite monochromated MoKα radiation (λ = 0.71073 Å). The structures were directly solved by a heavy-atom method and expanded using Fourier techniques in the CrystalStructure version 4.0 program package (Rigaku/MSC, The Woodlands, TX, USA). Selected crystallographic data are listed in Table 1. CCDC 1434210 and 1434211 for the data at 130 and 180 K, respectively, include the experimental details and full geometrical parameter tables. These data can be obtained free of charge via http://www.ccdc.cam.ac.uk/conts/retrieving.html.

3.3. Magnetic Measurements

The direct-current magnetic susceptibility of a polycrystalline specimen of $[Fe(L_H^{iPr})_2(NCS)_2]$ was measured on a SQUID magnetometer (MPMS-XL7, Quantum Design, San Diego, CA, USA) in a temperature range 10–300 K. The sample was held in a gelatin capsule. The magnetic response was corrected with diamagnetic blank data of the sample holder measured separately, and the diamagnetism of the sample itself was corrected using Pascal's constants [38].

4. Conclusions

The abrupt SCO with the hysteresis width of 13 K was recorded for $[Fe(L_H^{iPr})_2(NCS)_2]$. The crystal structures were determined at 130 and 180 K for the LS and HS phases, respectively. Although the space group and *Z* value were unchanged at both temperatures, the conformation isomerization of one out of four independent isopropyl groups was clearly demonstrated, where the rotation around the $C(sp^2)$–$C(sp^3)$ bond occurs during the SCO. Detailed temperature dependent crystallographic analysis afforded a clue to the thermal hysteresis. Therefore, such a model compound carrying relatively small alkyl group may be helpful to comprehend mechanisms of SCO hysteresis.

Acknowledgments

This work was financially supported from KAKENHI (JSPS/15H03793).

Author Contributions

N.M. participated in the preparation, X-ray structural analysis, and magnetic study. A.K. checked out the reproducibility in the X-ray diffraction results. T.I. designed the study and wrote the manuscript.

Conflicts of Interest

The authors declare no conflict of interest.

References

1. Gütlich, P., Goodwin, H.A., Eds. *Spin Crossover in Transition Metal Compounds I, II, and III*; Springer-Verlag: Berlin, Germany, 2004.
2. Gütlich, P.; Hauser, A.; Spiering, H. Thermal and optical switching of iron(II) complexes. *Angew. Chem. Int. Ed. Engl.* **1994**, *33*, 2024–2054.
3. Halcrow, M.A. *Spin-Crossover Materials: Properties and Applications*; John Wiley & Sons, Ltd.: Oxford, UK, 2013.
4. Craig, G.A.; Roubeau, O.; Aromi, G. Spin state switching in 2,6-bis(pyrazol-3-yl)pyridine (3-bpp) based Fe(II) complexes. *Coord. Chem. Rev.* **2014**, *269*, 13–31.
5. Munoz, M.C.; Real, J.A. Thermo-, piezo-, photo- and chemo-switchable spin crossover iron(II)-metallocyanate based coordination polymers. *Coord. Chem. Rev.* **2011**, *255*, 2068–2093.
6. Hayami, S.; Holmes, S.M.; Halcrow, M.A. Themed Issue: Spin-State Switches in Molecular Materials Chemistry. *J. Mater. Chem. C* **2015**, *3*, 7767–7977.
7. Real, J.A.; Gaspar, A.B.; Munoz, M.C. Thermal, pressure and light switchable spin-crossover materials. *Dalton Trans.* **2005**, doi:10.1039/B501491C.
8. Real, J.A.; Gaspar, A.B.; Niel, V.; Münoz, M.C. Communication between iron(II) building blocks in cooperative spin transition phenomena. *Coord. Chem. Rev.* **2003**, *236*, 121–141.
9. Aromi, G.; Barrios, L.A.; Roubeau, O.; Gamez, P. Triazoles and tetrazoles: Prime ligands to generate remarkable coordination materials. *Coord. Chem. Rev.* **2011**, *255*, 485–546.
10. Gamez, P.; Costa, J.S.; Quesada, M.; Aromi, G. Iron spin-crossover compounds: From fundamental studies to practical applications. *Dalton Trans.* **2009**, doi:10.1039/B908208E.
11. Halcrow, M.A. The spin-states and spin-transitions of mononuclear iron(ii) complexes of nitrogen-donor ligands. *Polyhedron* **2007**, *26*, 3523–3576.
12. Halcrow, M.A. Structure: Function relationships in molecular spin-crossover complexes. *Chem. Soc. Rev.* **2011**, *40*, 4119–4142.
13. Halcrow, M.A. Spin-crossover compounds with wide thermal hysteresis. *Chem. Lett.* **2014**, *43*, 1178–1188.
14. Hirosawa, N.; Oso, Y.; Ishida, T. Spin-crossover and light-induced excited spin-state trapping observed for an iron(II) complex chelated with tripodal tetrakis(2-pyridyl)methane. *Chem. Lett.* **2012**, *41*, 716–718.
15. Yamasaki, M.; Ishida, T. Spin-crossover thermal hysteresis and light-induced effect on iron(II) complexes with tripodal tris(2-pyridyl)methanol. *Polyhedron* **2015**, *85*, 795–799.
16. Chernyshov, D.; Hostettler, M.; Tornroos, K.W.; Burgi, H.-B. Ordering phenomena and phase transitions in a spin-crossover compound- uncovering the nature of the intermediate phase of $[Fe(2\text{-pic})_3]Cl_2 \cdot EtOH$. *Angew. Chem. Int. Ed.* **2003**, *42*, 3825–3830.

17. Miyazaki, Y.; Nakamoto, T.; Ikeuchi, S.; Saito, K.; Inaba, A.; Sorai, M.; Tojo, T.; Atake, T.; Matouzenko, G.S.; Zein, S.; *et al*. Spin crossover phenomenon accompanying order-disorder phase transition in the ligand of $[Fe^{II}(DAPP)(abpt)](ClO_4)_2$ compound (DAPP = bis(3-aminopropyl)(2-pyridylmethyl)amine, abpt = 4-amino-3,5-bis(pyridin-2-yl)-1,2,4-triazole) and its successive self-grinding effect. *J. Phys. Chem. B* **2007**, *111*, 12508–12517.
18. Guionneau, P.; Letard, J.-F.; Yufit, D.S.; Chasseau, D.; Bravic, G.; Goeta, A.E.; Howard, J.A.K.; Kahn, O. Structural approach of the features of the spin crossover transition in iron(II) compounds. *J. Mater. Chem.* **1999**, *9*, 985–994.
19. Hayami, S.; Shigeyoshi, Y.; Akita, M.; Inoue, K.; Kato, K.; Osaka, K.; Takata, M.; Kawajiri, R.; Mitani, T.; Maeda, Y. Reverse spin transition triggered by a structural phase transition. *Angew. Chem. Int. Ed.* **2005**, *117*, 4977–4981.
20. Yamasaki, M.; Ishida, T. Heating-rate dependence of spin-crossover hysteresis observed in an iron(II) complex having tris(2-pyridyl)methanol. *J. Mater. Chem. C* **2015**, *3*, 7784–7787.
21. Létard, J.-F.; Guionneau, P.; Codjovi, E.; Lavastre, O.; Bravic, G.; Chasseau, D.; Kahn, O. Wide thermal hysteresis for the mononuclear spin-crossover compound *cis*-bis(thiocyanato)bis[*N*-(2′-pyridylmethylene)-4-(phenylethynyl)anilino]iron(II). *J. Am. Chem. Soc.* **1997**, *119*, 10861–10862.
22. Letard, J.-F.; Guionneau, P.; Nguyen, O.; Costa, J.S.; Marcen, S.; Chastanet, G.; Marchivie, M.; Goux-Capes, L. A guideline to the design of molecular-based materials with long-lived photomagnetic lifetimes. *Chem. Eur. J.* **2005**, *11*, 4582–4589.
23. Ikuta, Y.; Ooidemizu, M.; Yamahata, Y.; Yamada, M.; Osa, S.; Matsumoto, N.; Iijima, S.; Sunatsuki, Y.; Kojima, M.; Dahan, F.; *et al*. A new family of spin crossover complexes with a tripod ligand containing three imidazoles: Synthesis, characterization, and magnetic properties of $[Fe^{II}H_3L^{Me}](NO_3)_2\cdot 1.5H_2O$, $[Fe^{III}L^{Me}]\cdot 3.5H_2O$, $[Fe^{II}H_3L^{Me}][Fe^{II}L^{Me}]NO_3$, and $[Fe^{II}H_3L^{Me}][Fe^{III}L^{Me}](NO_3)_2$ (H_3L^{Me} = tris[2-(((2-methylimidazol-4-yl)methylidene)amino)-ethyl]amine). *Inorg. Chem.* **2003**, *42*, 7001–7017.
24. Oso, Y.; Ishida, T. Spin-crossover transition in a mesophase iron(II) thiocyanate complex chelated with 4-hexadecyl-*N*-(2-pyridylmethylene)aniline. *Chem. Lett.* **2009**, *38*, 604–605.
25. Oso, Y.; Kanatsuki, D.; Saito, S.; Nogami, T.; Ishida, T. Spin-crossover transition coupled with another solid-solid phase transition for iron(II) thiocyanate complexes chelated with alkylated *N*-(di-2-pyridylmethylene)anilines. *Chem. Lett.* **2008**, *37*, 760–761.
26. Bondi, A. van der Waals volumes and radii. *J. Phys. Chem.* **1964**, *68*, 441–451.
27. Broeker, J.L.; Hoffmann, R.W.; Houk, K.N. Conformational analysis of chiral alkenes and oxonium ions: *Ab initio* molecular orbital calculations and an improved MM2 force field. *J. Am. Chem. Soc.* **1991**, *113*, 5006–5017.
28. Schaefer, T.; Sebastian, R.; Penner, G.H. Theoretical and experimental data on the internal rotatioinal potential in isopropylbenzene. *Can. J. Chem.* **1988**, *66*, 1495–1499.
29. Schaefer, T.; Parr, W.J.E.; Danchura, W. Concerning the barrier to internal rotation in isopropylbenzene in solution. *J. Mag. Reson.* **1977**, *25*, 167–170.
30. True, N.S.; Farag, M.S.; Bohn, R.K.; Madregor, M.A.; Radhakrishnan, J. Low-resolution microwave studies of substituted ethyl- and isopropylbenzenes. *J. Phys. Chem.* **1983**, *87*, 4622–4627.

31. Seredyuk, M.; Muñoz, M.C.; Castro, M.; Morcillo, T.R.; Gaspar, A.B.; Real, J.A. Unprecedented multi-stable spin crossover molecular material with two thermal memory channels. *Chem. Eur. J.* **2013**, *19*, 6591–6596.
32. Lakhloufi, S.; Guionneau, P.; Lemee-Cailleau, M.H.; Rosa, P.; Letard, J.-F. Structural phase transition in the spin-crossover complex $[Fe(ptz)_6](BF_4)_2$ studied by X-ray diffraction. *Phys. Rev. B* **2010**, doi:10.1103/PhysRevB.82.132104.
33. Craig, G.A.; Costa, J.S.; Roubeau, O.; Teat, S.J.; Aromí, G. Coupled crystallographic order-disorder and spin state in a bistable molecule: Multiple transition dynamics. *Chem. Eur. J.* **2011**, *17*, 3120–3127.
34. Khalil, M.; Marcus, M.A.; Smeigh, A.L.; McCusker, J.K.; Chong, H.H.W.; Schoenlein, R.W. Picosecond X-ray absorption spectroscopy of a photoinduced iron(II) spin crossover reaction in solution. *J. Phys. Chem. A* **2006**, *110*, 38–40.
35. Ortega-Villar, N.; Thompson, A.L.; Munoz, M.C.; Ugalde-Saldivar, V.M.; Goeta, A.E.; Moreno-Esparza, R.; Real, J.A. Solid- and solution-state studies of the novel μ-dicyanamide-bridged dinuclear spin-crossover system $\{[(Fe(bztpen))_2[\mu\text{-}N(CN)_2]\}(PF_6)_3 \cdot n H_2O$. *Chem. Eur. J.* **2005**, *11*, 1–15.
36. Weber, B.; Walker, F.A. Solution NMR studies of iron(II) spin-crossover complexes. *Inorg. Chem.* **2007**, *46*, 6794–6803.
37. Barth, P.; Schmauss, G.; Specker, H. Complexes of iron(II) with substituted 2-pyridinalphenylimines. *Z. Naturforsch. B* **1972**, *27b*, 1149–1154.
38. Kahn, O. *Molecular Magnetism*; VCH: Weinhein, Germany, 1993.